ELSEVIER

Polymer 42 (2001) 9193–9203

polymer

www.elsevier.com/locate/polymer

Experimental studies of stress–diffusion coupling in semi-dilute polymer solutions. I. 'Viscoelastic length' and viscoelastic effects on early stage spinodal decomposition

Nobuyuki Toyoda, Mikihito Takenaka, Shin Saito, Takeji Hashimoto*

Department of Polymer Chemistry, Graduate School of Engineering, Kyoto University, Kyoto 606-8501, Japan

Received 17 March 2001; received in revised form 29 March 2001; accepted 29 March 2001

Abstract

We investigated the viscoelastic effects on the early stage spinodal decomposition (SD) in semi-dilute polymer solutions where the coupling between stress and diffusion plays an important role. The so-called viscoelastic length, ξ_{ve}, within which the stress suppresses the growth of the concentration fluctuations, was quantitatively evaluated experimentally. The evaluated value was found out to be about 10 times larger than the radius of gyration of polymer. We measured the interdiffusion coefficient, the cooperative diffusion coefficient, the zero-shear viscosity, and the plateau modulus in the one phase region and evaluated ξ_{ve} independently from the SD experiment. The value ξ_{ve} obtained in the early stage SD agrees well with that estimated from the diffusion and viscoelasticity measurements, confirming the validity of the Doi–Onuki theory. © 2001 Elsevier Science Ltd. All rights reserved.

Keywords: Semi-dilute polymer solution; Spinodal decomposition; Viscoelastic length

1. Introduction

Dynamics of phase separation processes have been one of the most interesting subjects in chemical physics both from an experimental and theoretical point of view and widely investigated for various systems such as metal alloys, binary simple liquids, and polymer blends [1–5]. Recently, it has been found that the dynamical asymmetry between constituent components in mixtures and solutions causes a coupling between stress and diffusion that is due to an asymmetric stress division [6]. This coupling effect causes unique 'viscoelastic effects' on the phase separation process [7–10], shear-induced concentration fluctuations or phase separation in polymer solutions [11–15] and nonsingle-exponential decay in dynamic light scattering (DLS) for polymer solutions [16].

Doi and Onuki (DO) have accounted for this effect theoretically by formulating a time-dependent Ginzburg–Landau (TDGL) type equation which incorporates the dynamical coupling between stress and diffusion [6]. Onuki and Taniguchi further developed the linearized dynamical equation where they considered only a single relaxation process for the stress term in the TDGL equation to apply to the early stage spinodal decomposition (SD) [17]. Thus, both the dynamics of concentration fluctuations in phase separation processes in two phase systems as well as dynamics of the concentration fluctuations in one-phase systems depend not only on the thermodynamic force and transport coefficient in the system but also on the stress inhomogeneity arising from concentration fluctuations and its relaxation process. The dynamical asymmetry and viscoelastic effects are thought to play an important role in concentration fluctuations of polymer mixtures and solutions as well as other physical systems, e.g. gels, colloidal suspensions. Thus, a clarification of these effects is an important step towards the deeper understanding of the dynamics of concentration fluctuations in general complex fluid systems.

In this paper, we aim to explore the effects on SD in semi-dilute polymer solutions and to analyse the experimental results in the context of the DO theory. In this way, we will quantitatively clarify how the viscoelastic effects affect the growth rate of concentration fluctuations in a dynamically asymmetric system composed of polymer and solvent as dynamically asymmetric elements. In assessing the validity of the DO theory, we focus on the so called 'viscoelastic length', ξ_{ve}. ξ_{ve} characterizes the length over which the stress built-up (as a consequence of the growth of concentration fluctuations) and subsequent relaxation

* Corresponding author. Tel.: +81-75-753-5604; fax: +81-75-753-4864.
E-mail address: hashimoto@alloy.polym.kyoto-u.ac.jp (T. Hashimoto).

PII: S0032-3861(01)00393-7

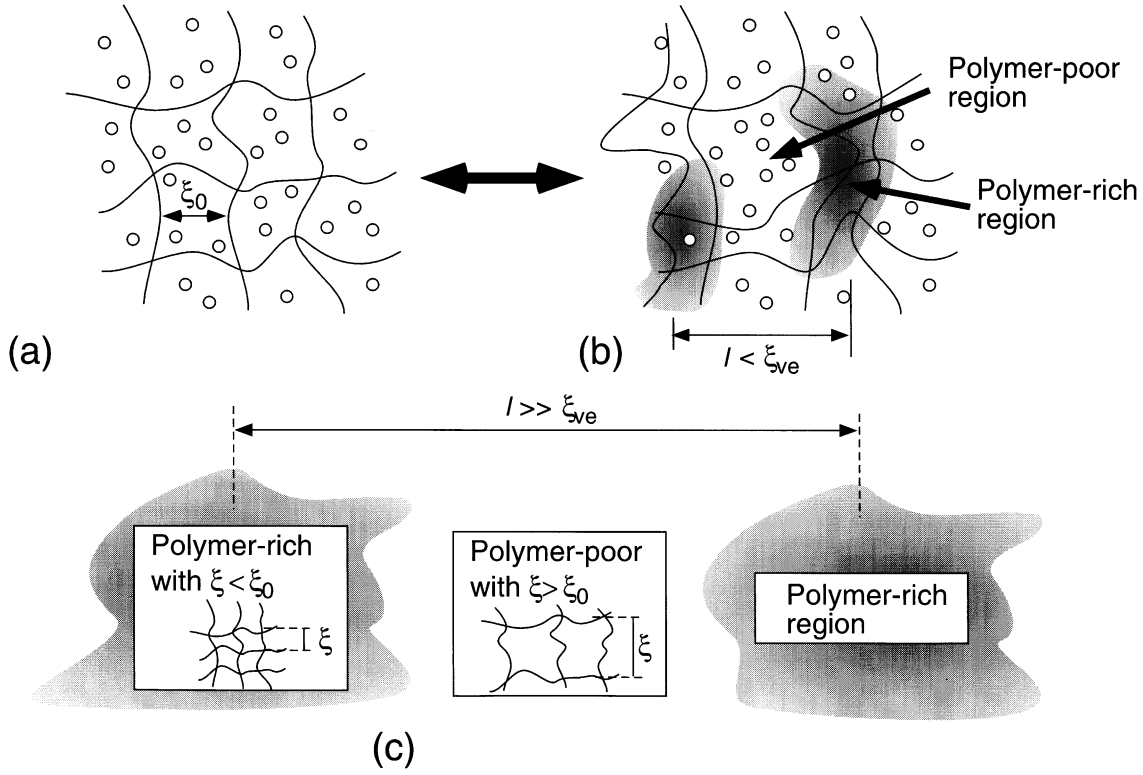

Fig. 1. Schematic representation of the concept of stress–diffusion coupling and the viscoelastic effects in polymer solutions. Semi-dilute solutions with relatively homogeneous concentration (a) before phase separation, and with concentration fluctuations at a short length scale (b) and at a larger length scale (c) after phase separation. ξ_0 designates an average mesh size for statistically homogeneous semi-dilute solution. In parts (b) and (c), the shaded regions designate polymer-rich with the average mesh size $\xi < \xi_0$, while the unshaded region designate polymer-poor regions with $\xi > \xi_0$. Parts (b) and (c) differ in the characteristic length l for the concentration fluctuations.

process suppresses the growth rate of the concentration fluctuations.

Fig. 1 attempts to show schematically the concept of stress–diffusion coupling, viscoelastic length, and the viscoelastic effects. Suppose that concentration fluctuations with a characteristic length l are developed, as shown in Fig. 1(b) and (c), from an entangled polymer solution with statistically homogeneous polymer concentration in Fig. 1(a). Note that in Fig. 1(a), ξ_0 is the average mesh size, the shaded and unshaded areas in Fig. 1(b) and (c) represent regions with higher and lower polymer concentrations with smaller and larger mesh sizes, respectively. If the growth rate of the concentration fluctuations Γ_l is faster than the relaxation rate of the entangled polymer networks Γ_n, the concentration fluctuations will build up local stress. Furthermore, its spatial variation, and the built-up stress will be relaxed at a rate Γ_n, which is characterized by viscoelastic properties of the system. The local variation of the stress field in the solution affects the free energy functional of the system and hence the diffusion processes of the system.

Thus stress–diffusion coupling occurs when $\Gamma_l > \Gamma_n$ and suppresses the dynamics of concentration fluctuations. If the length l is comparable with an average mesh size of the entangled polymer networks ξ_0 (as shown in Fig. 1(b)), this criterion should be fulfilled. However, for large length-scale concentration fluctuations (when $l \gg \xi_0$ as shown in Fig. 1(c)), Γ_l is extremely small and such fluctuations will be developed under a situation where the built-up stress is completely relaxed, hence involving no such stress–diffusion coupling.

Thus we can envision a screening length called the 'viscoelastic length' ξ_{ve} for the stress–diffusion coupling: If $l > \xi_{ve}$, the coupling is screened out, but if $l < \xi_{ve}$, it is relevant and is expected to become increasingly important with decreasing l, since $\Gamma_l \sim l^{-2}$ and local stress built-up and its inhomogeneity increase with decreasing l. Thus the coupling would affect the transport property of the system expressed by the Onsager kinetic coefficient $\Lambda(q)$. At large q (satisfying $q\xi_{ve} > 1$), this causes a suppression of $\Lambda(q)$ as q^{-2} as will be discussed in Section 2.2. $q(\sim l^{-1})$ is wave number of a Fourier mode of the concentration fluctuations that are detected by scattering experiments at a particular magnitude of scattering vector **q**,

$$q = (4\pi/\lambda)\sin(\theta/2) \tag{1}$$

with λ and θ being the wavelength of the incident beam and the scattering angle in the solutions, respectively.

It is striking to recognize that phase separation can be coupled by viscoelastic relaxation and hence the viscoelastic properties of the system. The research along this

line is fascinating, as it involves various fundamental problems in physical science, such as (i) nonequilibrium statistical mechanics of phase transition and structure formation in thermodynamically unstable systems, (ii) rheology, (iii) scattering and structural characterization, and (iv) polymer physics on semi-dilute polymer solutions.

In a separate short letter [18], we reported the SD process of semi-dilute polymer solutions with time-resolved light scattering (TRLS) experiments and evaluated ξ_{ve}. In addition to this analysis, we estimated ξ_{ve} also from measurements of the diffusion and viscoelastic properties of the same solutions as that used in the SD experiment in one phase region. We found that the value ξ_{ve} obtained in the early stage SD experiments agrees well with that estimated from the diffusion and viscoelasticity measurements. In an extension of the previous paper, we present here the results obtained at different temperatures and also details of the estimation procedure of ξ_{ve} from the diffusion and viscoelasticity measurements.

This paper consists of the following sections. We briefly give a theoretical background on our problem, including the Cahn–Hilliard–Cook (CHC) theory and DO theory in Section 2. We will show the experimental results on the SD process of the polymer solution in Section 4, after describing the experimental methods in Section 3. In Section 5, we will first evaluate ξ_{ve} both from the TRLS experiments and from the diffusion and viscoelastic measurements, and then compare the two results obtained independently. Finally, we will summarize our results in Section 6.

2. Theoretical background

2.1. Cahn–Hilliard–Cook theory

The description of the dynamics of phase separation processes in A/B binary mixtures is expressed by a nonlinear time-evolution equation based on time-dependent Ginzburg–Landau theory whereby the local concentration fluctuation $\delta\phi_A(\mathbf{r},t)$ at position $\mathbf{r}$ and time t is given by [19–21]:

$$\frac{\partial}{\partial t}\delta\phi_A(\mathbf{r},t) = \Lambda\nabla^2\mu(\mathbf{r},t) + \zeta(\mathbf{r},t) + (\text{HD term}), \tag{2}$$

where Λ is the Onsager kinetic coefficient, $\mu(\mathbf{r},t)$ is the local chemical potential, $\zeta(\mathbf{r},t)$ is the random thermal force term, and the HD term is concerned with the long-range hydrodynamic interactions [19–21]. $\delta\phi_A(\mathbf{r},t)$ is given by

$$\delta\phi_A(\mathbf{r},t) \equiv \phi_A(\mathbf{r},t) - \phi_{A0} \tag{3}$$

with $\phi_A(\mathbf{r},t)$ and ϕ_{A0} being, respectively, the volume fraction of component A at $\mathbf{r}$ and t, and the space-averaged $\phi_A(\mathbf{r},t)$. The random thermal force term can be expressed by the following fluctuation–dissipation relation [1]:

$$\langle\zeta(\mathbf{r},t)\zeta(\mathbf{r}',t')\rangle = -2k_BT\Lambda\nabla^2\delta(\mathbf{r}-\mathbf{r}')\delta(t-t'), \tag{4}$$

where k_B and T are, respectively, the Boltzmann constant and absolute temperature, and $\langle\ \rangle$ denotes the thermal average. If $\delta\phi_A(\mathbf{r},t)$ is small and the HD term can be neglected, Eq. (2) can be linearized in terms of $\delta\phi_A(\mathbf{r},t)$:

$$\frac{\partial}{\partial t}\delta\phi_A(\mathbf{r},t) = \Lambda\nabla^2(-r_0 - C\nabla^2)\delta\phi_A(\mathbf{r},t) + \zeta(\mathbf{r},t), \tag{5}$$

where C is a positive constant related to the nonlocality of interactions [22]. r_0 is a parameter related to thermodynamic driving force for phase separation which is defined to be positive in unstable region and increases with the quench depth.

By applying Fourier transformation to Eq. (5), we obtain

$$\frac{\partial}{\partial t}\delta\phi_A(q,t) = \Lambda(q)q^2(r_0 - Cq^2)\delta\phi_A(q,t) + \zeta(q,t), \tag{6}$$

where $\delta\phi_A(q,t)$ and $\zeta(q,t)$ are, respectively, the Fourier q-modes of ϕ_A and ζ. $\zeta(q,t)$ is given by [23]

$$\langle\zeta(q,t)\zeta(q',t')\rangle = 2k_BT\Lambda(q)q^2\delta(t-t')(2\pi)^3\delta(q+q'). \tag{7}$$

We can solve Eq. (5) to obtain scattered intensity as a function of q and t, $I(q,t)[\sim\langle|\delta\phi_A(q,t)|^2\rangle]$,

$$I(q,t) = I(q,\infty) + [I(q,0) - I(q,\infty)]\exp[2R(q)t], \tag{8}$$

where $I(q,0)$, $I(q,\infty)$, and $R(q)$ are, respectively, $I(q,t)$ at $t=0$, the virtual structure factor due to the random thermal force effects, and the growth rate of $\delta\phi_A(q,t)$. $R(q)$ is given by

$$R(q) = \Lambda(q)q^2(r_0 - Cq^2), \tag{9a}$$

$$R(q) = \Lambda(0)q^2(r_0 - Cq^2) \ \text{ at } q \ll R_g^{-1}, \tag{9b}$$

where R_g is radius of gyration of polymers. At $q \ll R_g^{-1}$, it is expected that $\Lambda(q)$ is governed by the diffusion of centres of mass of polymer coils, so that $\Lambda(q) = \Lambda(0)$, a constant independent of q. Thus the plot of $R(q)/q^2$ vs. q^2 should be linear at $q \ll R_g^{-1}$. This linearized theory is called Cahn–Hilliard–Cook theory (CHC theory) and it is well confirmed [24–30] that the dynamics of the early stage SD can be approximated by the CHC theory.

2.2. Doi–Onuki theory for spinodal decomposition in dynamically asymmetric systems

Doi and Onuki have taken the viscoelastic effects into account by formulating the TDGL type dynamical equation, which incorporates the dynamical coupling between stress and diffusion [6]. According to the DO theory, the dynamics of phase separation processes in A/B binary mixtures is

described by

$$\frac{\partial}{\partial t}\delta\phi_{\rm A}(\mathbf{r},t) = \Lambda\nabla\cdot[\nabla\mu(\mathbf{r},t) - \alpha\nabla\cdot\vec{\sigma}(\mathbf{r},t)] + \zeta(\mathbf{r},t) + (\text{HD term}), \tag{10}$$

where α and $\vec{\sigma}$ are, respectively, the dynamical asymmetric parameter and the local stress of the system. For polymer solutions, $\alpha = 1/\phi_{\rm A0}$, where $\phi_{\rm A0}$ is the space-averaged volume fraction of the polymer in the solution. If $\delta\phi_{\rm A}(\mathbf{r},t)$ is small and the HD term can be neglected, the linearized dynamical equation for $\delta\phi_{\rm A}(q,t)$ is given by [17],

$$\frac{\partial}{\partial t}\delta\phi_{\rm A}(q,t) = \Lambda(q)q^2(r_0 - Cq^2)\delta\phi_{\rm A}(q,t) - \Lambda(q)\alpha Z(q,t) + \zeta(q,t), \tag{11}$$

where $Z(q,t)$ is the Fourier component of $Z(\mathbf{r},t)$ given by

$$Z(\mathbf{r},t) \equiv \nabla\cdot\nabla\cdot\vec{\sigma}(\mathbf{r},t). \tag{12}$$

By linearizing the stress term $Z(q,t)$ for small $\delta\phi_{\rm A}(q,t)$, we obtain

$$Z(q,t) = \frac{4\alpha q^2}{3}\int_0^t {\rm d}t' G(t-t')\frac{\partial}{\partial t'}\delta\phi_{\rm A}(q,t'), \tag{13}$$

where $G(t)$ is the relaxation function for modulus and expressed by a sum of moduli for fundamental relaxation processes:

$$G(t) = \sum_{i=1}^{n} G_i \exp(-t/\tau_i) \tag{14}$$

with G_i and τ_i being strength and relaxation time of the ith relaxation process of the stress, where $\tau_1 > \tau_2 \cdots > \tau_n$. Substituting Eqs. (13) and (14) into Eq. (11), we obtain

$$\frac{\partial}{\partial t}\delta\phi_{\rm A}(q,t) = \Lambda(0)q^2(r_0 - Cq^2)\delta\phi_{\rm A}(q,t) - \frac{4\Lambda(0)q^2}{3\phi_{\rm A0}^2} \times \int_0^t {\rm d}t' G(t-t')\frac{\partial}{\partial t'}\delta\phi_{\rm A}(\mathbf{q},t') + \zeta(\mathbf{q},t) \tag{15}$$

at $q \ll 1/R_{\rm g}$, where $\Lambda(q) = \Lambda(0)$. The following is worth noting: The CHC theory [first term in RHS of Eq. (15)] predicts the concentration fluctuations grow at $q \leq (r_0/C)^{1/2}$ for the thermodynamic unstable solutions but the growth rate is suppressed due to existence of the second term in RHS of Eq. (15); the larger the q value, the larger the suppression.

If $R(q)^{-1}$ is larger than the longest relaxation time τ_1 in $G(t)$ (i.e. the stress relaxation occurs much faster than the concentration fluctuations), we can set $\partial\delta\phi_{\rm A}(q,t')/\partial t' = \partial\delta\phi_{\rm A}(q,t)/\partial t$, so that Eq. (15) reduces to

$$\left(1 + \frac{4\Lambda(0)\sum_{i=1}^{n} G_i\tau_i}{3\phi_{\rm A0}^2}q^2\right)\frac{\partial}{\partial t}\delta\phi_{\rm A}(q,t) = \Lambda(0)q^2(r_0 - Cq^2)\delta\phi_{\rm A}(q,t) + \zeta(q,t). \tag{16}$$

Therefore the change in $I(q,t)$ with time is described by the same form as that in Eq. (6) and hence in Eq. (8), except for the fact that $\Lambda(0)$ in Eq. (9b) should be replaced by a q-dependent Onsager kinetic coefficient defined hereafter as $\Lambda_{\rm eff}(q)$,

$$\Lambda_{\rm eff}(q) = \frac{\Lambda(0)}{1 + \xi_{\rm ve}^2 q^2}. \tag{17}$$

The q-dependence of the Onsager coefficient originates from the viscoelastic length $\xi_{\rm ve}$ defined by

$$\xi_{\rm ve} = \left(\frac{4\Lambda(0)\sum_{i=1}^{n} G_i\tau_i}{3\phi_{\rm A0}^2}\right)^{1/2} = \left(\frac{4\Lambda(0)\eta_0}{3\phi_{\rm A0}^2}\right)^{1/2}, \tag{18}$$

where η_0 is zero-shear viscosity of the solution. Thus $R(q)$ in Eq. (9b) should be replaced by

$$R(q) = \Lambda_{\rm eff}(q)q^2(r_0 - Cq^2) \tag{19}$$

2.3. Doi–Onuki theory for dynamic structure factor in dynamically asymmetric systems

Let us discuss the dynamics of the concentration fluctuations in the one phase solution as elucidated by the dynamic structure factor $S(q,t)$, which can be measured with dynamic light scattering (DLS) [31]. Applying Laplace transformation to Eq. (15) with respect to t, we obtain

$$\delta\phi_{\rm A}(q,\omega) = \frac{1 + (4\Lambda(0)q^2G(\omega)/3\phi_{\rm A0})}{R(q) + {\rm i}\omega + (4\Lambda(0)q^2G(\omega)/3\phi_{\rm A0})}\delta\phi_{\rm A}(q,0), \tag{20}$$

where $\delta\phi_{\rm A}(\mathbf{r},\omega)$ and $G(\omega)$ are, respectively, the Laplace-transformed $\delta\phi_{\rm A}(q,t)$ and $G(t)$, respectively. $S(q,t)$ is given by

$$S(q,t) = \frac{\langle\delta\phi_{\rm A}(q,0)\delta\phi_{\rm A}^*(q,t)\rangle}{\langle\delta\phi_{\rm A}(q,0)\delta\phi_{\rm A}^*(q,0)\rangle}, \tag{21}$$

where $*$ denotes the complex conjugate. Thus the Laplace-transformed $S(q,t)$, $S(q,\omega)$, is given by

$$S(q,\omega) = \frac{1 + (4\Lambda(0)q^2G(\omega)/3\phi_{\rm A,0})}{R(q) + {\rm i}\omega + (4\Lambda(0)q^2G(\omega)/3\phi_{\rm A0})}. \tag{22}$$

When $G(t)$ is expressed by Eq. (14), the inverse Laplace

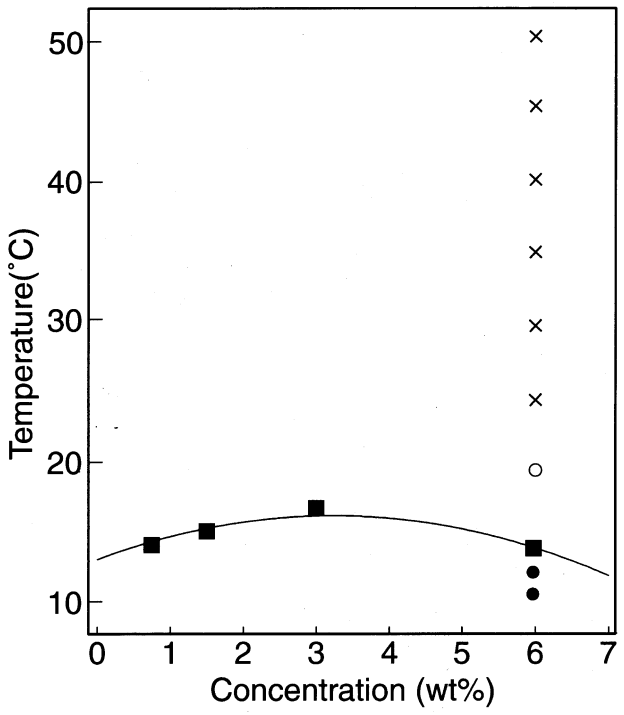

Fig. 2. Cloud point curve of PS/DOP solution. The filled circles and open circles, respectively, indicate the temperatures after and before quench for the TRLS experiment described in the text, while crosses indicate the temperatures where the viscoelastic and DLS measurements were conducted.

transformation of Eq. (22) gives

$$S(q,t) = \sum_{i=1}^{m} S_i(q)\exp[-\Gamma_i(q)t], \tag{23}$$

where Γ_i and S_i are the q-dependent relaxation rate and the relaxation intensity of the ith relaxation process, respectively. Γ_i and S_i have the following relationship with interdiffusion coefficient D and cooperative diffusion coefficient D_c:

$$\sum_{i=1}^{m} S_i(q)\Gamma_i(q) = Dq^2 \tag{24}$$

and

$$\sum_{i=1}^{m} \Gamma_i(\mathbf{q}) = D_c\mathbf{q}^2 + \sum_{j=1}^{n} \tau_j^{-1}, \tag{25}$$

where D and D_c have the following two relationships,

$$D = \Lambda(0)r_0, \tag{26}$$

and

$$D_c = D + \frac{4\Lambda(0)}{3\phi_{A0}^2}\sum_{i=1}^{n} G_i. \tag{27}$$

Here $\sum_{i=1}^{n} G_i$ corresponds to the rubbery plateau modulus G_N of the solution. Thus, D and D_c, respectively, can be estimated from the slope of a plot of $\sum_{i=1}^{m} S_i\Gamma_i$ vs. q^2, and from the slope of a plot of $\sum_{i=1}^{m} \Gamma_i$ vs q^2 [31]. $\sum_{i=1}^{m} S_i\Gamma_i$ can be estimated from the first cumulant of $S(q,t)$, $K_1(q) = -[\partial \ln S(q,t)/\partial t]_{t\to 0}$, since $\sum_{i=1}^{m} S_i\Gamma_i = K_1$.

From Eqs. (18) and (27), we obtain

$$\xi_{ve}^2 = \frac{(D_c - D)\eta_0}{G_N}. \tag{28}$$

Thus, we can estimate ξ_{ve} from DLS and viscoelastic measurements.

3. Experimental method

3.1. Sample preparation

The polymer used here is polystyrene (PS) with the weight-averaged molecular weight M_w of 5.48×10^6 and the polydispersity index $M_w/M_n = 1.15$, where M_n denotes the number-averaged molecular weight. Dioctyl phthalate (DOP) was used as a solvent. The Θ temperature of the solution is 22°C. The concentration of PS used was 6.0 wt% which is 6.7 times larger than the overlap concentration. The solution was prepared by dissolving PS and DOP in excess methylene chloride and by completely evaporating methylene chloride. Fig. 2 shows the cloud point curve of the PS/DOP solution. The PS/DOP solution has an upper critical solution temperature type phase diagram and the 6 wt% solution has cloud point of 13.8°C.

3.2. Time-resolved light scattering measurement

We quenched the solution from 20.0°C (one phase region as shown by the open circle in Fig. 2) to 10.8 and 12.3°C (where the solution was in thermodynamically unstable region; filled circles in Fig. 2) and then measured the change in the scattered intensity $I(q,t)$ as a function of q and time t during the phase separation process of the solution with time-resolved light scattering (TRLS) technique with a He–Ne laser as a light source. The range of scattering angle covered was from 2 to 65° in air, corresponding to the range of q from 1.02×10^{-3} to 9.5×10^{-3} nm^{-1}. The scattered intensity was corrected for the fluctuation of the incident beam and the turbidity of the sample [32].

3.3. Dynamic light scattering measurement

We measured DLS for the same solution as that used for the TRLS measurements in one phase region with an ALV-5000® instrument using an Ar^+ ion laser as a light source. The scattering angle for DLS measurement was varied from 30 to 150°. The temperature range covered for DLS varied from 25 to 50°C with a temperature step of 5°C (crosses in Fig. 2). The scattering cells were precision 10 mm diameter NMR tubes. The sample cells were immersed in a (15 cm diameter) cylindrical bath filled with index matching liquid (toluene) for the DLS measurement.

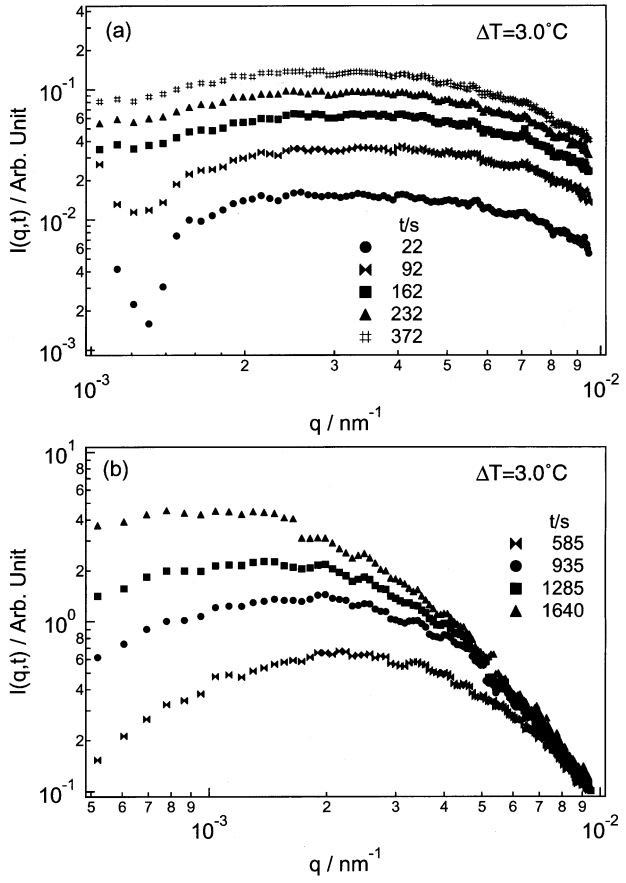

Fig. 3. Changes in the light scattering profiles with time during (a) an early stage and (b) later stage phase-separation process after the quench from $T = 20.0$ to 10.8°C. ΔT is quench depth from the cloud point temperature (13.8°C).

3.4. Viscoelastic measurement

The viscoelastic properties were investigated with stress relaxation measurements (SRM) and steady-shear viscosity measurements (SVM) in the one phase region using the same solution as that employed for the TRLS measurement. The covered temperature range for SRM and SVM was identical to that used for DLS. A rheometer (Rheometrics ARES®) with a fluid bath temperature control was used for SRM and SVM with the cone-and-plate fixture. The strain used in SRM, 0.5, was within the linear viscoelastic range. The SVM frequency ranged from 0.001 to 10 s^{-1}.

4. Results

Fig. 3 shows the change in $I(q,t)$ during the phase separation process after the onset of the quench from 20.0 to 10.8°C. In the early stage of phase separation shown in Fig. 3(a), the scattering peak appears at a particular q-value defined as q_m, $q_m \cong 3.0 \times 10^{-3}$ nm^{-1}, and the scattered intensity increases with time in the observed q-range, while the q_m value remains nearly unchanged with t. This change in $I(q,t)$ is similar to that in the early stage spinodal decomposition in polymer blends or dilute polymer solutions, except for the fact that the peaks here are much broader than others. In this work, we focus on the early stage phase separation behaviour and hence we analyze the data with CHC theory. Similarly to other systems, the peak position shifts towards the smaller q-region after the early stage as shown in Fig. 3(b), indicating that the coarsening process occurs. However, the scattered intensity in higher q-regions increases more slowly than that at lower q-regions, so that the scattered intensity distribution becomes broader with time.

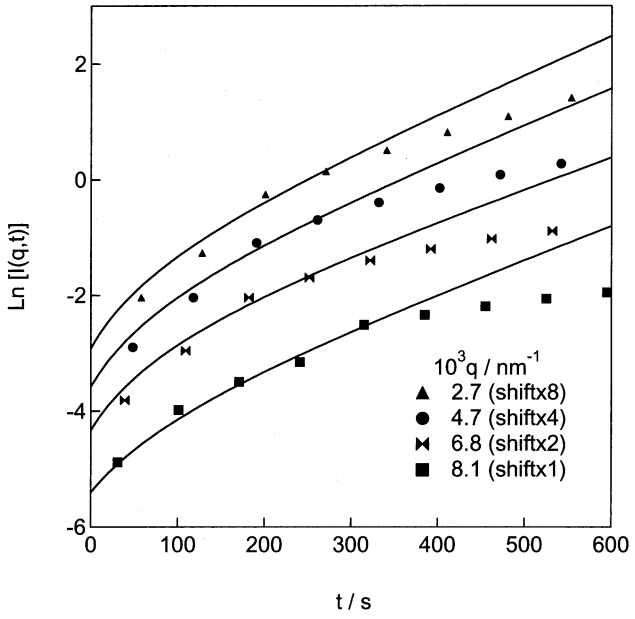

Fig. 4. The semi-logarithmic plot of $I(q,t)$ vs. t at various fixed qs after the quench. The solid lines show the best-fit of $I(q,t)$ (symbols) with Eq. (8) using nonlinear regression.

Fig. 4 shows the semi-logarithmic plot of $I(q,t)$ vs. t at various fixed qs after the onset of the quench. The CHC theory predicts that the change in $I(q,t)$ with time in the early stage SD can be described by Eq. (8). Thus, we checked whether or not our early stage data corresponded to CHC behaviour by conducting a nonlinear fit of this data to Eq. (8), using $I(q,\infty)$, $I(q,0)$ and $R(q)$ as adjustable parameters at each q value. We were able to fit the data well and obtained the growth rate $R(q)$. The data deviate from the fitting curves at large t because the nonlinear term becomes nonnegligible as a consequence of the increase in the amplitude of the concentration fluctuations. Actually, a remarkable slow down in the rate of intensity growth can be observed in the later stage of $t \gtrsim 350$ s.

Fig. 5 shows the q-dependence of $R(q)$ at 10.8 (×) and 12.3°C (○). The plot of $R(q)$ vs. q has a maximum at $q = 3.0 \times 10^{-3}$ nm^{-1} at 10.8°C which agrees with the peak position in $I(q,t)$. In Fig. 5, $R(q)$ at $T = 12.3$°C with the peak at $q = 4.0 \times 10^{-3}$ nm^{-1} is also shown [18]. The behaviour of $R(q)$ at both temperatures show a similar tendency, though

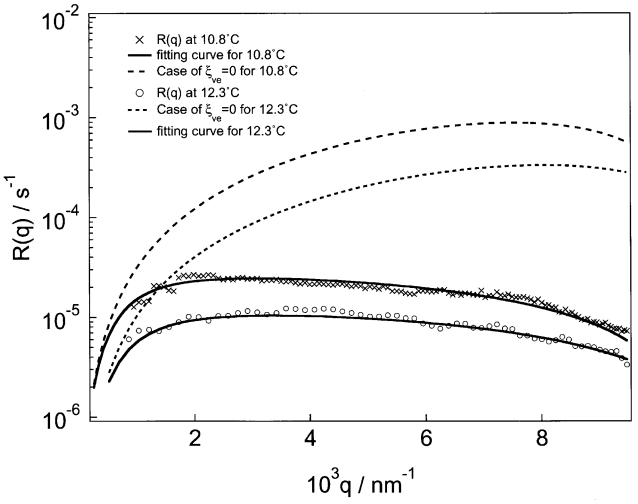

Fig. 5. Semi-logarithmic plots of $R(q)$ (crosses at 10.8°C and circles at 12.3°C) vs. q. The solid lines indicate the $R(q)$ calculated by using Eqs. (17) and (19) with $\xi_{ve} = 1.04 \times 10^3$ nm at $T = 10.8$°C and $\xi_{ve} = 9.5 \times 10^2$ nm at $T = 12.3$°C, while the two broken lines indicate the corresponding fictitious curves of $R(q)$ for the case of $\xi_{ve} = 0$.

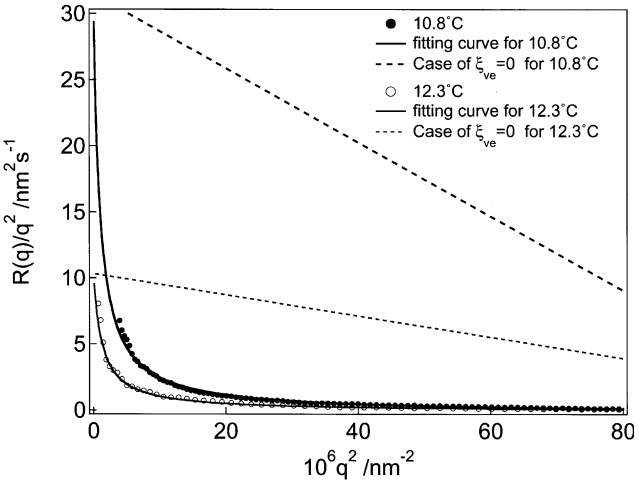

Fig. 6. $R(q)/q^2$ is plotted as a function of q^2. The solid lines are the best fit of the results (filled circles at 10.8°C and open squares at 12.3°C) with Eqs. (17) and (19) with $\xi_{ve} = 1.04 \times 10^3$ and 9.5×10^2 nm, respectively, while the two broken lines are the corresponding fictitious cases with $\xi_{ve} = 0$.

$R(q)$ at $T = 10.8$°C is larger because of the deeper quench, indicating that the phase separation at these temperatures is in thermodynamic-control regime.

According to the CHC theory, the q-dependence of $R(q)$ is given by Eqs. (9a) and (9b). As discussed already, Eq. (9b) is applied to our experimental condition. Thus the plot of $R(q)/q^2$ vs. q^2 should be linear. However, as shown in Fig. 6, the plots of $R(q)/q^2$ vs. q^2 for the both quenches (represented by filled circles and open squares) do not show the linear relationship but rather a quite remarkable nonlinear behaviour as characterized by a large downward curvature, in contrast to the CHC prediction and the previous results [24–30].

We investigated possibility that this $R(q)/q^2$ behaviour originated from the viscoelastic effects, by analyzing the data with the DO theory as will be discussed in the Section 5.1.

5. Discussion

5.1. Test of DO theory

We were able to fit the plot of $R(q)/q^2$ vs. q^2 with Eqs. (17) and (19), using r_0, C, and ξ_{ve} as floating parameters, as shown by the solid line in Fig. 6. The viscoelastic length ξ_{ve} obtained is 1.04×10^3 nm at $T = 10.8$°C and 9.0×10^2 nm at $T = 12.3$°C. Fig. 7 shows comparisons of the experimental (symbols) and theoretical results (dash-dot line and solid line for the results at 12.3 and 10.8°C, respectively) on the q-dependence of $\Lambda_{eff}(q)$. $\Lambda_{eff}(q)$ has a q^{-2} power law dependence at high q, indicating that the viscoelastic effects strongly suppress the growth rate of the concentration fluctuations in this q regime and can cause the downward curvature in the plot shown in Fig. 6. It is found that $\Lambda_{eff}(q)$ at $T = 10.8$°C is more suppressed than that at $T = 12.3$°C, since ξ_{ve} is larger at the lower temperature. The broken lines in Figs. 5–7 present the fictitious case where the viscoelastic effects on $R(q)$ could be ignored ($\xi_{ve} = 0$). Comparing the two cases, the actual growth rate $R(q)$ is much smaller, and the degree of suppression increases with increasing q (or $q\xi_{ve}$). The peak position of the fictitious $R(q)$ with $\xi_{ve} = 0$ is 7.5×10^{-3} nm^{-1} at 10.8°C and 8.0×10^{-3} nm^{-1} at 12.3°C; about twice as large as those of the respective actual $R(q)$. This indicates that the viscoelastic effects affect not only the growth rate of the concentration fluctuations but also the wavelength of the initial periodic structure developed in the early stage SD.

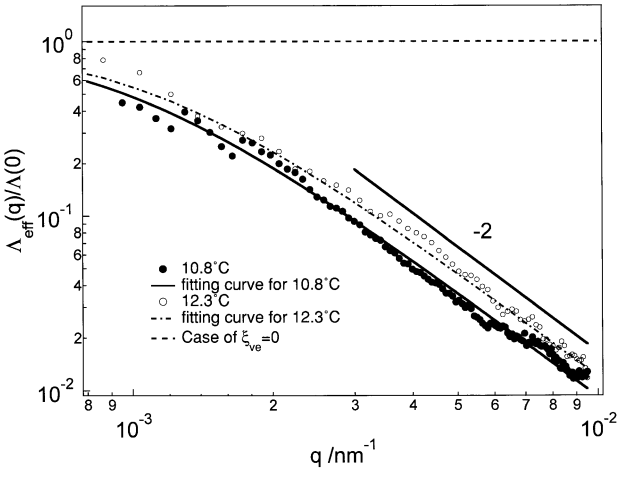

Fig. 7. $\Lambda_{eff}(q)/\Lambda(0)$ is plotted as a function of q. The solid line indicates $1/(1 + q^2\xi_{ve}^2)$ with $\xi_{ve} = 1.04 \times 10^3$ nm at $T = 10.8$°C and $\xi_{ve} = 9.5 \times 10^2$ nm at $T = 12.3$°C, while the horizontal broken line is the fictitious case with $\xi_{ve} = 0$.

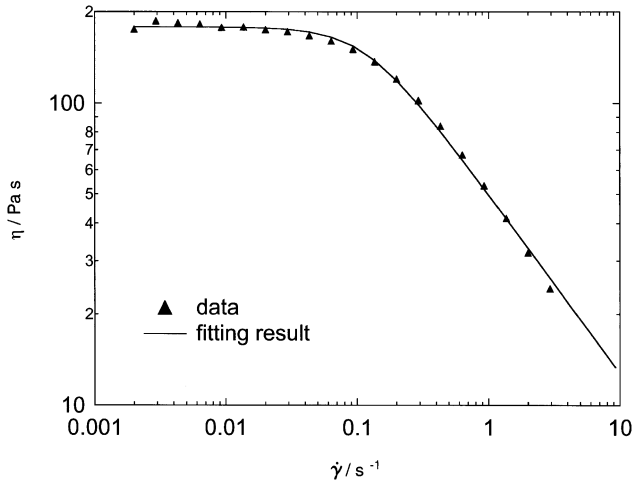

Fig. 8. η plotted as a function of $\dot{\gamma}$ at 50°C. The solid line is the best fit results with Eq. (29).

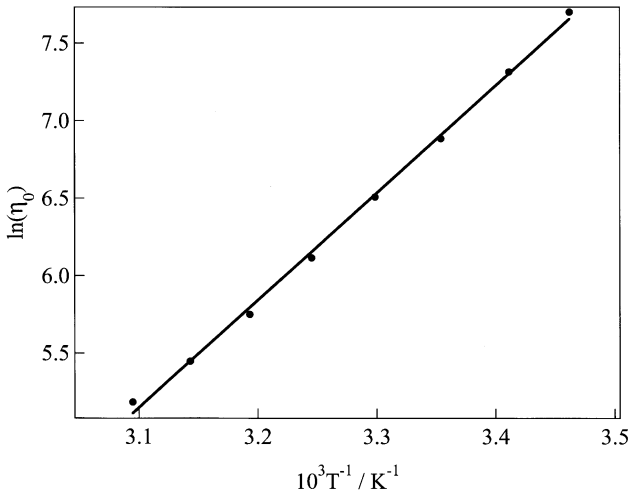

Fig. 9. η_0 is plotted as a function of inverse of absolute temperature. The solid line is the best fit of the results (filled circles) with an Arrhenius type equation (Eq. (30)).

5.2. Independent estimation of ξ_{ve} from DLS and viscoelastic measurements

In Section 5.1, we estimated the viscoelastic length ξ_{ve} from time-evolution studies of the concentration fluctuations in the early stage SD process using Eqs. (17) and (19). Here, we confirm validity of ξ_{ve} thus estimated by comparing it to ξ_{ve} values obtained from other independent experiments. As discussed in Section 2.3, ξ_{ve} can be also evaluated using Eq. (28). For this purpose, η_0, G_N, D, and D_c must be measured. However we cannot directly measure them at 10.8 and 12.3°C, because the solution is in the two phase region at these temperatures. Therefore, we measured them at various temperatures in one phase region and extrapolated the respective values to those at 10.8 and 12.3°C in order to assess ξ_{ve}s at 10.8 and 12.3°C.

5.2.1. Estimation of η_0

We obtained the temperature dependence of η_0 from SVM of the solution. Fig. 8 shows a typical shear rate ($\dot{\gamma}$) dependence of viscosity η at a given temperature (50°C). At lower $\dot{\gamma}$s, η becomes constant, while the shear thinning can be observed at higher $\dot{\gamma}$. We were able to fit the data on η vs. $\dot{\gamma}$ at a measured temperature with the Carreau Model [33]:

$$\eta = \eta_0[1 + (\tau_m\dot{\gamma})^2]^{-a}, \tag{29}$$

using η_0, τ_m, and a as floating parameters, where τ_m and a are, respectively, the longest relaxation time and the power-law index. Fig. 9 shows the temperature dependence of η_0 thus evaluated. η_0 was expressed by the following Arrhenius type equation in units of Pa·s:

$$\eta_0 = 8.51 \times 10^{-8}\exp[(6.91 \times 10^3)/T]. \tag{30}$$

5.2.2. Estimation of G_N

We estimated G_N from the SRM measurement. Fig. 10 shows the typical behaviour of the solution shear modulus $G(t)$ with time for a given temperature (of 50°C). We analyzed $G(t)$ with Procedure-X [34] and found $G(t)$ was well-fitted with the sum of exponential functions (Eq. (14)). The steady-state compliance J_e^0 was calculated from $G(t)$ as 7.46×10^{-2} Pa^{-1} at 50°C using

$$J_e^0 = \frac{\sum_{i=1}^{n} G_i\tau_i^2}{\left(\sum_{i=1}^{n} G_i\tau_i\right)^2}. \tag{31}$$

We estimated $G_N = 26.8$ Pa from the following empirical relationship [35]:

$$G_N J_e^0 = 2.0. \tag{32}$$

In this way G_N was determined as a function of T, though the data is not shown.

5.2.3. Estimation of D and D_c from DLS

Fig. 11 typically shows $S(q,t)$ of the solution at $q = 2.0 \times 10^{-2}$ nm^{-1}, 2.8×10^{-2} nm^{-1}, and 3.2×10^{-2} nm^{-1}, and at $T = 50$°C. $S(q,t)$ was evaluated from the autocorrelation function $g(q,t)$ of the scattered intensity by using the standard correlation spectroscopy. In order to obtain D, we estimated the first cumulant K_1 from the plot of $\ln[S(q,t)]$ vs. t over the early time regime. Fig. 12 typically shows K_1 of the solution (at 50°C) plotted as a function of q^2. The data shows a linear relationship with a zero intercept (Eq. (24)). This behaviour was observed at other temperatures as well and we later estimate the temperature dependence of D (Fig. 15).

In order to obtain the distribution of Γ_i and the value $\sum_{i=1}^{m}\Gamma_i$, we analyzed $S(q,t)$ with CONTIN [36]. Fig. 13 shows S_i plotted as a function of Γ_i at various q values and at $T = 50$°C. We calculated $\sum_{i=1}^{m}\Gamma_i$ from these

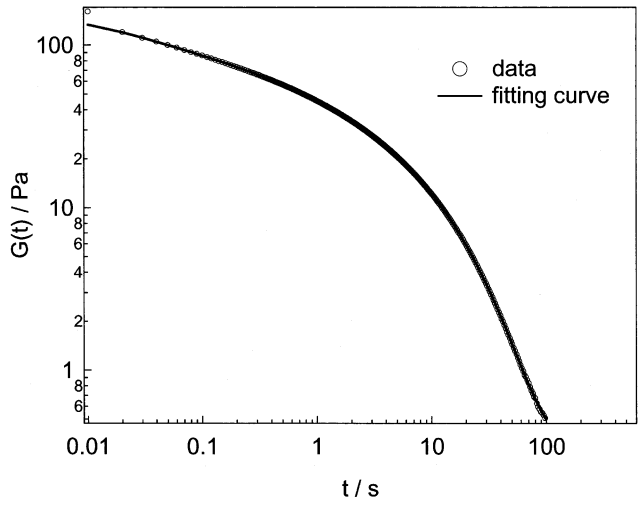

Fig. 10. $G(t)$ of the solution at 50°C double-logarithmically plotted as a function of t. The solid line indicates the best fit obtained with the Procedure-X.

distribution and the value was plotted as a function of q^2 in Fig. 14. D_c was determined from the slope of the linear plot (Eq. (25)). This procedure was repeated for other temperatures, and the temperature dependence of D_c is shown in Fig. 15 (filled squares).

The temperature dependence of $D_c - D$ was also determined and found to have the following equation:

$$D_c - D = 3.00 \times 10^2 \exp(-8.24 \times 10^3/T), \quad (33)$$

as shown in Fig. 15. From the temperature dependence of η_0 and $D - D_c$, and G_N, we estimated the viscoelastic length ξ_{ve} using Eq. (28). Fig. 16 shows the weak temperature dependence of ξ_{ve}. The open circles in Fig. 16 show ξ_{ve} obtained from TRLS experiment during the SD processes. The extrapolated values (solid line) from one phase region agree well with that obtained from the dynamics of early

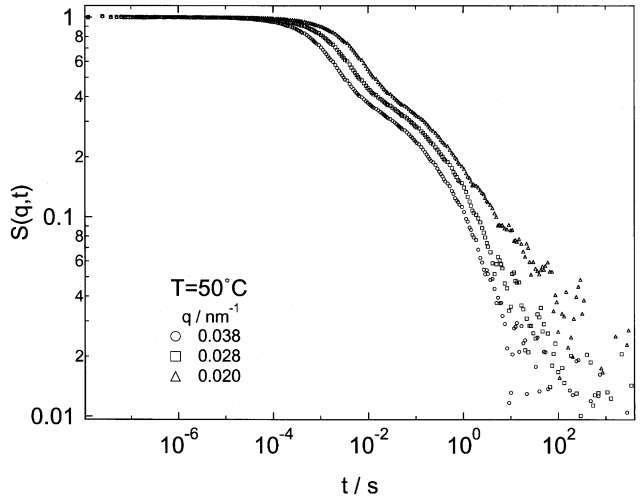

Fig. 11. $S(q,t)$ at 50°C is double-logarithmically plotted as a function of t.

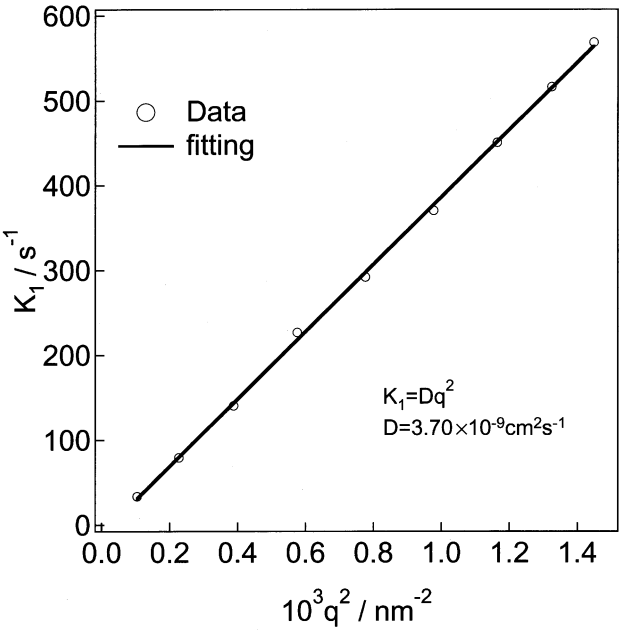

Fig. 12. K_1 at 50°C plotted as a function of q^2. The solid line is the best fit of the results.

stage SD. This agreement is the first clear-cut confirmation of the fact that the DO theory can be used to describe the dynamics of the phase separation process in dynamically asymmetric binary systems.

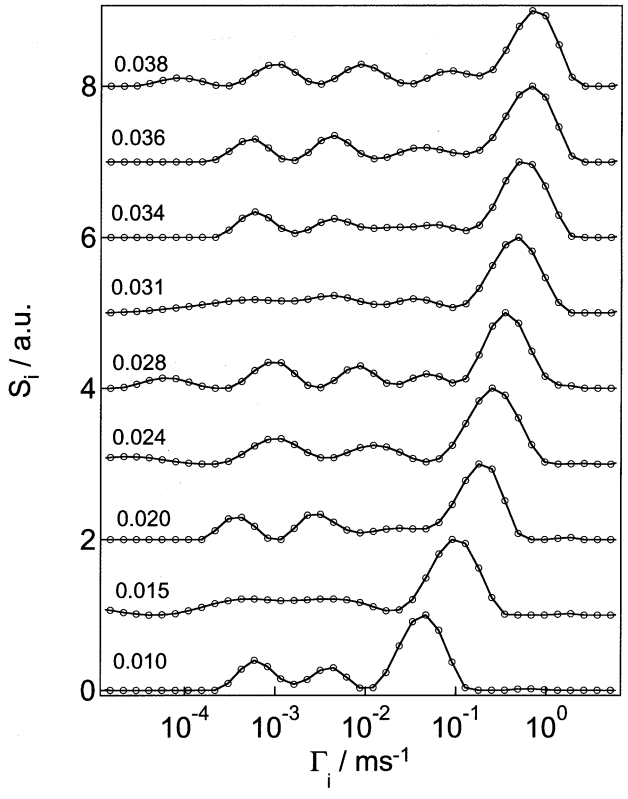

Fig. 13. Semi-logarithmic plot of S_i vs. Γ_i at various qs and at $T = 50$°C. Each plot is shifted by a factor of 1.

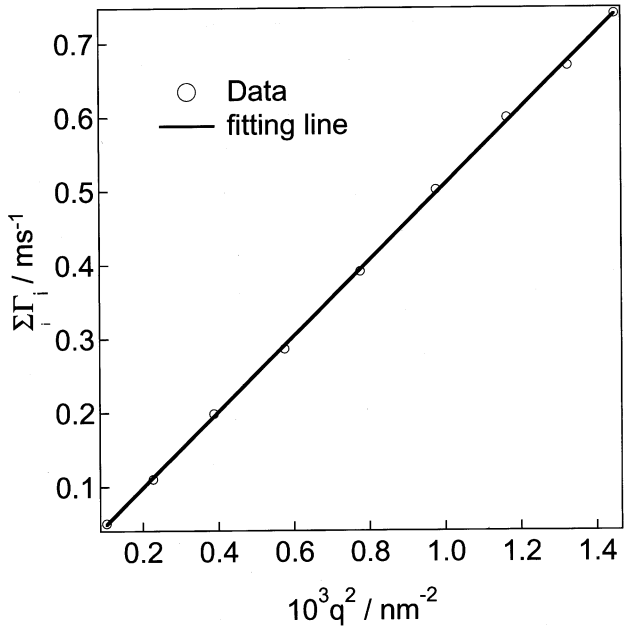

Fig. 14. $\sum_{i=1}^{m} \Gamma_i$ plotted as a function of q^2 at 50°C. The solid line is the best fit of the results.

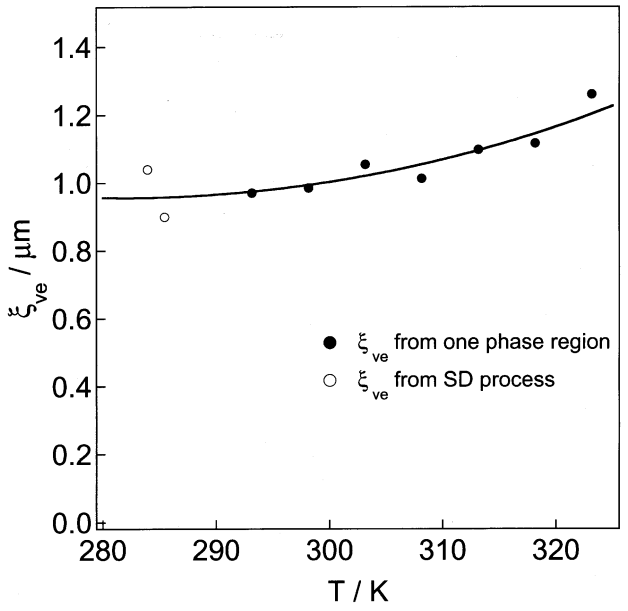

Fig. 16. Temperature dependence of ξ_{ve} in the one phase region (filled circles), as estimated from the DLS and viscoelastic measurements, and in the two-phase region (open circles), as estimated from the dynamics of the SD process, respectively.

6. Conclusion

We investigated the viscoelastic effects on the dynamics of early stage SD in PS/DOP solutions where dynamical asymmetry between polymer and solvent gives rise to stress–diffusion coupling. We found that this effect strongly suppresses the growth rate of the concentration fluctuations at length scales smaller than the viscoelastic length ξ_{ve} and that the length ξ_{ve} can be very large, about 10 times as large as R_g. We measured the interdiffusion coefficient, the cooperative diffusion coefficient, the zero-shear viscosity, and the plateau modulus at various temperatures in the one phase region in order to estimate ξ_{ve} as a function of temperature. ξ_{ve} values obtained in this manner at various temperatures can be extrapolated to the temperatures where the SD experiments were conducted. The extrapolated values agree well with those calculated from the analysis of the early stage SD, confirming validity of the DO theory.

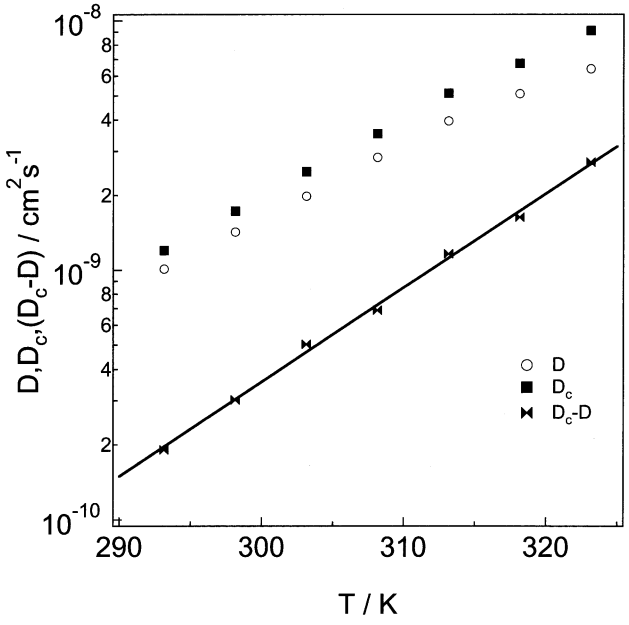

Fig. 15. $\ln D$, $\ln D_c$, and $\ln D_c - D$ plotted as a function of absolute temperature. The solid line is the best fit of the results (symbols) (Eq. (33)).

Acknowledgements

This work is financially supported in part by a Grant-in-Aid for Scientific Research (under Grant No. 12640392(C)) from the Ministry of Education, Science, and Culture, Japan. This work is also partially supported by the national project, which has been entrusted to the Japan Chemical Innovation Institute (JCII) by the New Energy and Industrial Technology Development Organization (NEDO) under MITI's Program for the Scientific Technology Development for Industries that Creates New Industries.

References

[1] Gunton JD, San Miguel M, Sahni PS. Phase Transitions 1983;8:269.
[2] Hashimoto T. Phase Transitions 1988;12:47.
[3] Hashimoto T. In: Komura S, Furukawa H, editors. Dynamics of ordering processes in condensed matter. New York: Plenum Publishing Corporation, 1988. p. 421.
[4] Binder K. In: Haasen P, editor. Phase transformations in materials,

Material science and technology, vol. 5. Weinheim: VCH, 1990. p. 405. Series editied by R.W. Cahn, P. Haasen, E.J. Kramer.
[5] Hashimoto T. In: Thomas EL, editor. Structure and properties of polymers, Material science and technology, Vol. 12. Weinheim: VCH, 1993. p. 252. Series edited by R. W. Cahn, P. Haasen, E.J. Kramer.
[6] Doi M, Onuki A. J Phys II (Fr) 1992;2:1631.
[7] Tanaka H. Phys Rev Lett 1993;71:3158.
[8] Tanaka H. J Chem Phys 1994;100:5323.
[9] Tanaka H. Phys Rev Lett 1996;76:787.
[10] Tanaka H. Phys Rev E 1997;56:4451.
[11] Hashimoto T, Fujioka K. J Phys Soc Jpn 1991;60:356.
[12] Dixon PK, Pine DJ, Wu X-L. Phys Rev Lett 1992;68:2239.
[13] Hashimoto T, Kume T. J Phys Soc Jpn 1992;61:1839.
[14] Kume T, Hattori T, Hashimoto T. Macromolecules 1997;30:427.
[15] Saito S, Matsuzaka K, Hashimoto T. Macromolecules 1999;32:4879.
[16] Wu X-L, Pine DJ, Dixon PK. Phys Rev Lett 1991;66:2408.
[17] Onuki A, Taniguchi T. J Chem Phys 1997;106:5761.
[18] Takenaka M, Toyoda N, Saito S, Hashimoto T. submitted to Phys Rev Lett 2001.
[19] Kawasaki K. Prog Theor Phys 1977;57:826.
[20] Kawasaki K, Ohta T. Prog Theor Phys 1978;59:362.
[21] Koga T, Kawasaki K. Phys Rev A 1991;44:R817.
[22] Cahn JW. J Chem Phys 1965;42:93.
[23] Binder K. J Chem Phys 1983;79:6387.
[24] Hashimoto T, Kumaki J, Kawai H. Macromolecules 1983;16:641.
[25] Snyder HL, Meakin P. J Chem Phys 1983;79:5588.
[26] Izumitani T, Hashimoto T. J Chem Phys 1985;83:3694.
[27] Hashimoto T, Itakura M, Hasegawa H. J Chem Phys 1986;85:6118.
[28] Bates FS, Wiltzius P. J Chem Phys 1989;91:3258.
[29] Higgins JS, Fruitwala HA, Tomlins PE. Br Polym J 1989;21:247.
[30] Takenaka M, Hashimoto T. J Chem Phys 1992;96:6177.
[31] Einaga Y, Karube D. Polymer 1998;40:157.
[32] Stein RS, Keane JJ. J Polym Sci 1955;13:21.
[33] Bird RB, Armstrong RC, Hassager O. Dynamics of polymeric liquids. New York: Wiley, 1977.
[34] Tobolsky AV, Murakami K. J Polym Sci 1959;40:443.
[35] Onogi S, Masuda T, Kitagawa K. Macromolecules 1970;3:109.
[36] Provencher SW. Macromol Chem 1979;180:201.